Acta Pharmaceutica Sinica B 2019;9(3):537–544

Chinese Pharmaceutical Association
Institute of Materia Medica, Chinese Academy of Medical Sciences

Acta Pharmaceutica Sinica B

www.elsevier.com/locate/apsb
www.sciencedirect.com

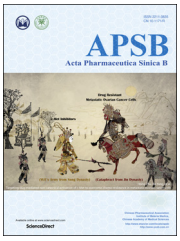

ORIGINAL ARTICLE

Aurone derivatives as Vps34 inhibitors that modulate autophagy

Guodong Li[a,†], Joshua William Boyle[b,†], Chung-Nga Ko[c,†], Wu Zeng[d], Vincent Kam Wai Wong[d], Jian-Bo Wan[a], Philip Wai Hong Chan[b,e,*], Dik-Lung Ma[c,*], Chung-Hang Leung[a,*]

[a]*State Key Laboratory of Quality Research in Chinese Medicine, Institute of Chinese Medical Sciences, University of Macau, Macau 999078, China*
[b]*School of Chemistry, Monash University, Clayton 3800, Australia*
[c]*Department of Chemistry, Hong Kong Baptist University, Hong Kong 999077, China*
[d]*State Key Laboratory of Quality Research in Chinese Medicine, Macau University of Science and Technology, Macau 999078, China*
[e]*Department of Chemistry, University of Warwick, Coventry CV4 7AL, UK*

Received 26 December 2018; received in revised form 19 January 2019; accepted 23 January 2019

KEY WORDS

Autophagy;
Natural products;
Vps34;
Inhibitor;
Structure-based virtual screening;
Vesicle trafficking;
Heart or liver damage;
Aurone derivative

Abstract We report in this study the identification of a natural product-like antagonist (**1a**) of Vps34 as a potent autophagy modulator *via* structure-based virtual screening. Aurone derivative **1a** strongly inhibited Vps34 activity in cell-free and cell-based assays. Significantly, **1a** prevents autophagy in human cells induced either by starvation or by an mTOR inhibitor. *In silico* modeling and kinetic data revealed that **1a** could function as an ATP-competitive inhibitor of Vps34. Moreover, it suppressed autophagy *in vivo* and without inducing heart or liver damage in mice. **1a** could be utilized as a new motif for more selective and efficacious antagonists of Vps34 for the potential treatment of autophagy-related human diseases.

Abbreviations: CETSA, cellular thermal shift assay; Co-IP, co-immunoprecipitation; DMEM, Dulbecco's modified Eagle's medium; DMSO, dimethyl sulfoxide; EBSS, Earle's balanced salt solution; ELISA, enzyme-linked immunosorbent assay; FBS, fetal bovine serum; PE, phosphatidylethanolamine; PI, phosphatidylinositol; PI3K, phosphoinositide 3-kinase; PI3P, phosphatidylinositol 3-phosphate; PS, phosphatidylserine

*Corresponding authors.
E-mail addresses: phil.chan@monash.edu (Philip Wai Hong Chan), edmondma@hkbu.edu.hk (Dik-Lung Ma), duncanleung@um.edu.mo (Chung-Hang Leung).
†These authors made equal contributions to this work.

Peer review under responsibility of Institute of Materia Medica, Chinese Academy of Medical Sciences and Chinese Pharmaceutical Association.

https://doi.org/10.1016/j.apsb.2019.01.016

1. Introduction

Autophagy acts as a stress response pathway against pathologic stresses, and also maintains proper function in cells by increasing the turnover of proteins and organelles and degrading damaged cytoplasmic components[1,2]. Defective autophagy is implicated in the development of maladies, such as diabetes, myopathy, neurodegeneration, liver disease, cancer, infection and immune disease[3–6]. Vps34, a catalytic subunit of phosphatidylinositol 3-kinase (PI3K) class III, mediates endocytosis as well as autophagosome–autolysosome creation so as to regulate autophagy and maintain cellular homeostasis[7,8]. Among the components of the autophagy machinery, Vps34 is the only class III kinase responsible for generating phosphatidylinositol 3-phosphate (PI3P) that mediates the start of autophagosome biogenesis[9]. Vps34 also plays an essential role in heart and liver function and its complete suppression in mammals can cause hepatomegaly, hepatosteatosis, and cardiomegaly[10,11]. Therefore, it is important to discover novel small molecule Vps34 modulators that can provide new opportunities for drug discovery and help understand the molecular mechanisms of autophagy, but without triggering the aforementioned heart and liver side effects.

As the C-terminus region of Vps34 binds to ATP, targeting the ATP-binding pocket of Vps34 is a potential approach for the discovery of novel Vps34 inhibitors[12]. However, it is far more difficult to identify Vps34 ATP-competitive inhibitors compared to class I PI3K inhibitors due to the smaller size of the Vps34 ATP-binding pocket[13–15]. Several ATP-competitive inhibitors of Vps34 have been reported in the literature, including SAR405[16], Vps34-IN1[17], and 3-methyladenine (3-MA)[18]. However, the potential hepatotoxicity and cardiotoxicity (or lack thereof) of those Vps34 inhibitors have so far not been demonstrated.

Natural products have long been regarded as a rich source of structural motifs for drug discovery[19–22]. Advances in virtual screening methodologies have allowed large numbers of natural products or natural products-derived compounds to be screened *in silico* with a dramatically reduction in costs when compared to traditional high-throughput screening[23,35,36,37,38]. We report herein the structure-based discovery of a novel and potent natural products-like Vps34 inhibitor as an autophagy modulator that does not damage the heart or liver in mice.

2. Results and discussion

2.1. Screening and structure-based optimization of small molecules as Vps34 inhibitors

The X-ray structure of Vps34 complexed with SAR405 (PDB: 4OYS) was used to construct a molecular model for our investigations[24]. A total of 90,000 natural products and natural

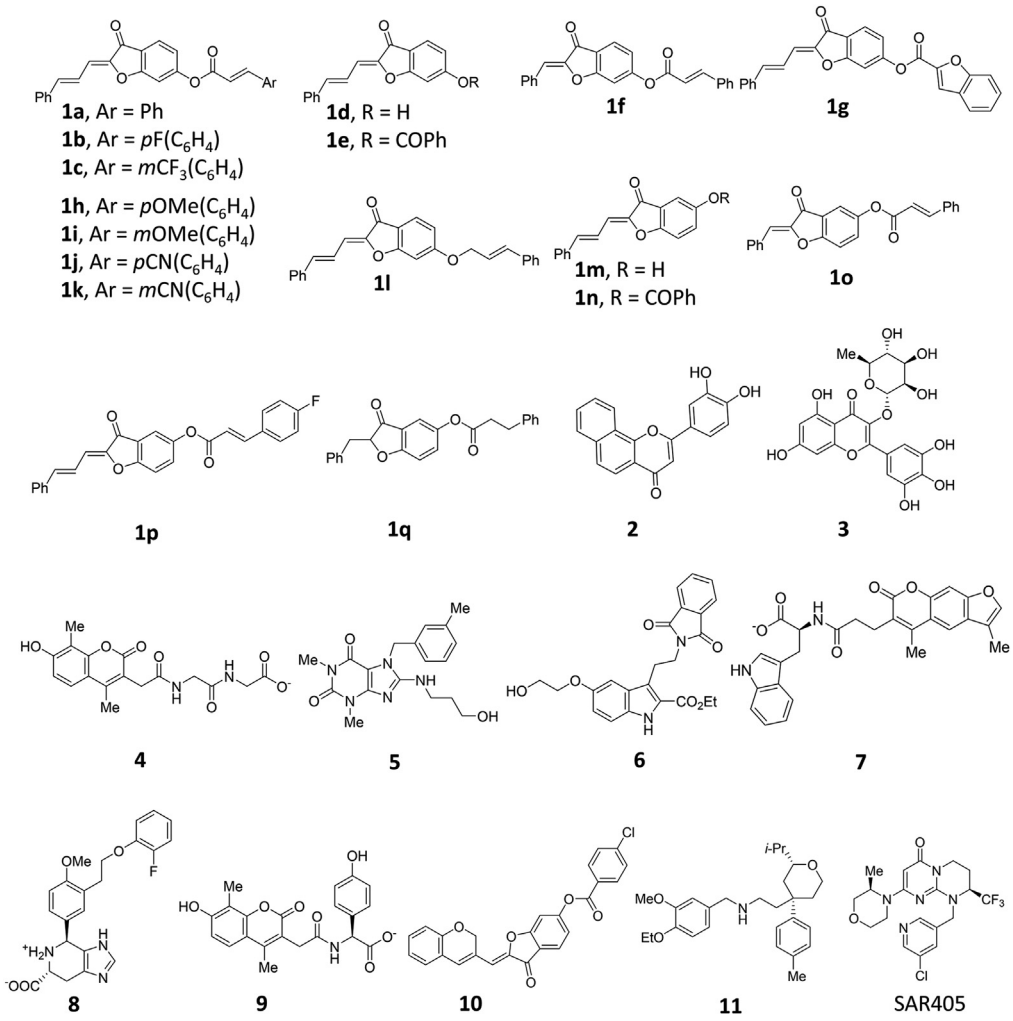

Figure 1 Chemical structures of compounds **1a–1q**, **2–11** and SAR405.

products-derived structures were docked into the Vps34–ATP site of Vps34 *in silico* using the ICM-Pro (3.6-1d) docking algorithm. Eleven compounds **1a** and **2–11** (Fig. 1) exhibited Gibbs free energy (ΔG) changes of lower than −30.0 kJ/mol, and were shortlisted for further biological testing.

An *in vitro* enzyme-linked immunosorbent assay (ELISA) was employed to detect the inhibitory effects of compounds (**1a**, **2–11**) on Vps34 kinase activity. Aurone derivative **1a** displayed the highest inhibition of Vps34 activity, with 79.6% reduction in luminescence activity at 100 nmol/L (Fig. 2). Compounds **3**, **4**, **8**, **10** and **11** showed moderate inhibitory activity in this assay, while little or no activity were exhibited by compounds **2**, **5–7**, and **9**. Notably, **1a** showed higher potency than SAR405, a known potent and selective Vps34 inhibitor[24]. A dose analysis was subsequently carried out to quantitate the efficacy of the aurone derivative **1a** at inhibiting Vps34 activity. The results showed that aurone derivative **1a** inhibited Vps34 in a concentration-dependent fashion with an IC_{50} of 7.6 nmol/L (Supporting Information Fig. S1), while SAR405 exhibited an IC_{50} value of 38 nmol/L under similar conditions. Compound **1a** also exhibit selectivity toward Vps34 over other PI3Ks isoforms, including p110α/p85α ($IC_{50} > 1000$ nmol/L), p110β/p85α ($IC_{50} > 1000$ nmol/L), p120γ (IC_{50} *ca.* 1000 nmol/L), and p120δ/p85α ($IC_{50} > 1000$ nmol/L) using ELISA (Supporting Information Fig. S2). Moreover, kinetic analysis showed that like SAR405, aurone derivative **1a** acts as an ATP-competitive inhibitor of Vps34 in a manner similar to that of SAR405 (Supporting Information Fig. S3). The lowest-scoring binding mode of **1a** in the ATP binding pocket of Vps34 is shown in Fig. 3. A high degree of shape complementarity is observed between the aurone derivative and the ATP binding pocket of Vps34, suggesting that this protein–ligand interaction could be stabilized by significant hydrophobic interactions. The side-chain carbonyl oxygen group of the aurone derivative **1a** is calculated to hydrogen bond with the side-chain of Asp761 along with the furanone carbonyl group forming similar hydrogen bonding interactions with the backbone amide motif of Ile685.

2.2. *Structure–activity relationships*

Inspired by the promising activity of aurone derivative **1a**, a series of derivatives were synthesized to study the structure–activity

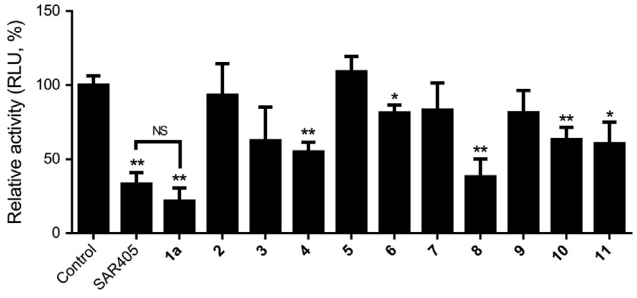

Figure 2 Compounds **1a**, **2–11** (100 nmol/L) inhibit the activity of Vps34 as determined by an ELISA assay. Error bars represent the standard deviations of results obtained from three independent experiments. Data are expressed as means ± SD ($n=3$). P values were calculated using a two-sided t-test. $^{*}P < 0.05$, $^{**}P < 0.01$ compounds *vs* control, NS (not significant, $P > 0.05$) **1a** *vs* SAR405.

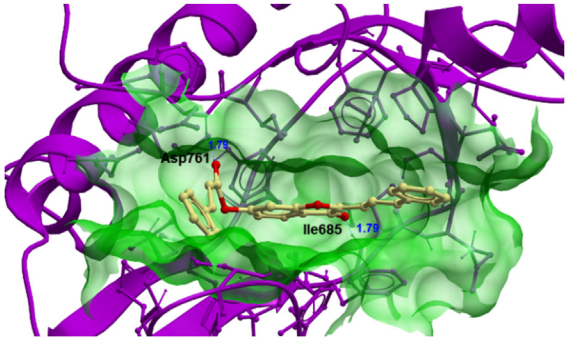

Figure 3 Top view of aurone derivative **1a** bound to the VPS34 generated by molecular docking. Vps34 (PDB: 4OYS) is depicted as a space-filling representation showing carbon (yellow), oxygen (red) atoms. The binding pocket of the Vps34 is represented as a translucent green surface (for interpretation of the references to color in this figure legend, the reader is referred to the web version of this article).

relationships (SAR) surrounding this scaffold. Analogues **1b–1g** retained the 3(2*H*)-benzofuranone core of **1a**, but varied in the nature of the substituents attached at the 2- and 6-positions (Fig. 1). In the ELISA assay, **1a** was again the most potent inhibitor of Vps34 out of all the analogues (Supporting Information Fig. S4). Considering those results, preliminary SAR could be determined. After compound **1a**, the second most potent molecule was **1g**, suggesting that a pendant benzofuran group at the 6-position could be mildly tolerated in place of the styrene group. However, converting the ester group at C6 into a hydroxy group (as in **1d**) led to the abolishment of activity. Adding fluorine atoms to the C2 pendant phenyl ring (as in **1b** and **1c**) was also undesirable for anti-Vps34 potency.

In the next round of screening, a series of further analogues (**1h–1q**) were synthesized. Interestingly, having a nitrile group at the *para* position (as in **1j**) completely abolished activity, whereas a nitrile group at the *meta* position (as in **1k**) produced significant activity. This suggests that steric effects around the C2 pendant ring may be important determinants of activity. Adding a fluorine atom to the C5 pendant group of **1o** (giving **1p**) led to a further weakening of activity. Finally, reducing the C6 ester carbonyl group of **1a** to methylene (as in **1l**) led to a significant decrease of activity.

2.3. *Aurone derivative **1a** affects vesicle trafficking in cellulo*

Recent studies have shown that Vps34 can regulate the expression level of p62, which is negatively correlated with autophagy[25,26]. Hence, the level of p62 in human cervical cancer HeLa cells treated with aurone derivative **1a** was evaluated. This was first confirmed by using an MTT assay that showed the aurone derivative to be only moderately cytotoxic towards HeLa, which gave an IC_{50} of 35 μmol/L (Supporting Information Fig. S6). The cytotoxicity of compound **1a** was further evaluated in three other cell lines, including a human breast adenocarcinoma cell line (MCF-7), a human hepatic cell line (LO2), and a human embryonic kidney cell line (HEK293T) using the MTT assay. **1a** also showed moderate cytotoxicity to MCF-7, LO2, and HEK293T cell lines with IC_{50} values of > 100, 25.12, and 37.15 μmol/L (Supporting Information Fig. S7), respectively. Encouragingly, aurone derivative **1a** (at 0.3–10 μmol/L) induced a dose-dependent increase in p62 in HeLa cells as revealed through Western blotting

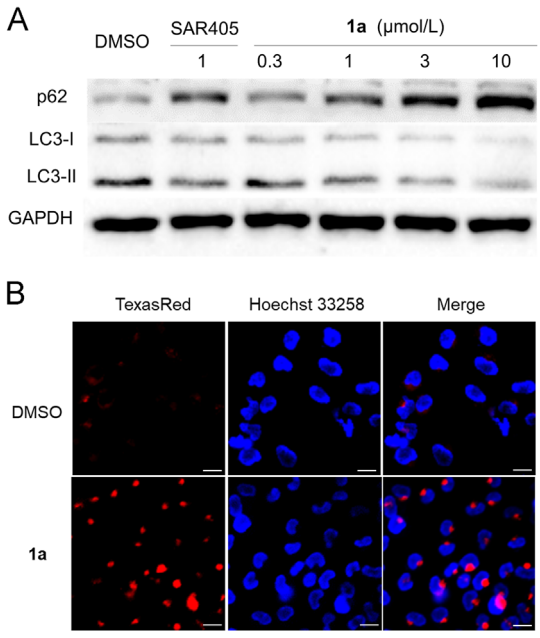

Figure 4 Effect of aurone derivative **1a** on Vps34 activity *in cellulo*. (A) The level of p62 in HeLa cells treated with **1a** was detected by Western blotting. (B) Effect of aurone derivative **1a** on vesicle trafficking in HeLa cells. HeLa cells were pretreated with **1a** (10 μmol/L) for 24 h before cell imaging. Scale bar = 20 μm.

(Fig. 4A and Supporting Information Fig. S8). This result suggests that **1a** could suppress autophagy by inhibiting Vps34 activity. In this assay, the aurone derivative **1a** showed comparable activity to the positive inhibitor SAR405. The difference in *in vitro* and *in cellulo* activities between compound **1a** and SAR405 could be due to multiple factors, such as differences in cell absorption or metabolism[27,28]. We also examined the effect of **1a** on vesicle trafficking, which is an important biological function of Vps34[29]. HeLa cells were stained with the lysosomal probe Lyso-Tracker Red and Hoechst 33258 in the presence of **1a** before imaging. Many large red spots were observed in the **1a**-treated HeLa cells (Fig. 4B), indicating the formation of late-endosomal compartments. By comparison, no such red spots were observed in untreated cells. These results reveal that aurone derivative **1a** can suppress vesicle trafficking presumably by inhibiting the activity of Vps34 *in cellulo*.

2.4. *Aurone derivative **1a** engages Vps34 in cellulo*

A cellular thermal shift assay (CETSA) was conducted to confirm binding affinity of Vps34 by aurone derivative **1a**[30]. An obvious shift of *ca.* 5 °C in the Vps34 melting curve was observed when 10 μmol/L of **1a** was present, which indicated that **1a** could engage with and stabilize Vps34 in cell lysates (Fig. 5A and B). We also performed co-immunoprecipitation experiments to investigate whether **1a** could affect the formation of Vps34 complexes. Aurone derivative **1a** did not disrupt the interaction between Vps34 with its partner proteins Vps15 and Beclin 1 (Supporting Information Fig. S9). Furthermore, the levels of Beclin 1 were not significantly increased after aurone derivative **1a** treatment in HeLa cells as revealed by Western blotting (Supporting Information Fig. S10), indicating **1a** could regulate Vps34-Beclin 1 complexes without affecting the levels of Beclin 1.

Moreover, a knockdown assay was performed to further verify the targeting of Vps34 by **1a**. HeLa cells were preincubated with siVps34 to silence Vps34 expression (Supporting Information Fig. S11). As expected, knockdown of Vps34 resulted in an accumulation of p62 (Fig. 5C). However, the aurone derivative was less able to further increase p62 accumulation in Vps34 knockdown cells compared with control cells (Fig. 5D). Collectively, our results indicate that **1a** could target and engage Vps34 in cells, and that its inhibition is not mediated through disruption of the Vps34 complex. This is consistent with the molecular modeling and kinetic analysis performed above suggesting that aurone derivative **1a** targeted the ATP-binding pocket of Vps34.

2.5. ***1a** prevents starvation- and rapamycin-induced autophagy*

Vps34 has a key function in both starvation and mTOR inhibitor-induced autophagy[5]. Therefore, we examined the effect of aurone derivative **1a** on autophagy induced by nutrient stress or mTOR inhibition. GFP-LC3 HeLa cells stably expressing GFP-LC3, a marker of autophagosomes, were used to monitor autophagy

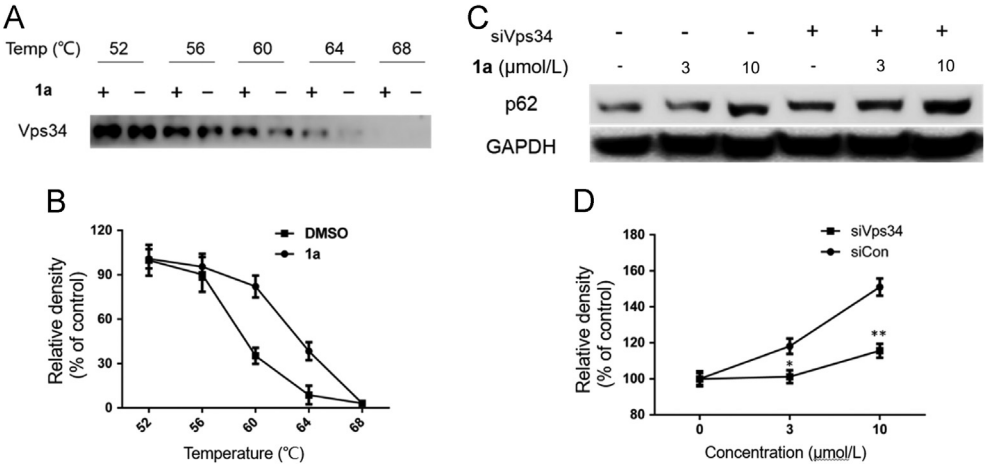

Figure 5 Aurone derivative **1a** selectively engages Vps34 as its prime cellular target. (A) Stabilization of Vps34 in HeLa cell lysates by **1a**. (B) Densitometry analysis of the cell-based Western blot showing **1a**-mediated stabilization of Vps34. (C) p62 levels in HeLa cells with or without knockdown Vps34 in the presence or absence of **1a**. (D) Densitometry analysis of p62 levels on the Western blot. Data are expressed as mean ± SD ($n=3$). $^{*}P < 0.05$, $^{**}P < 0.01$ **1a** *vs* DMSO.

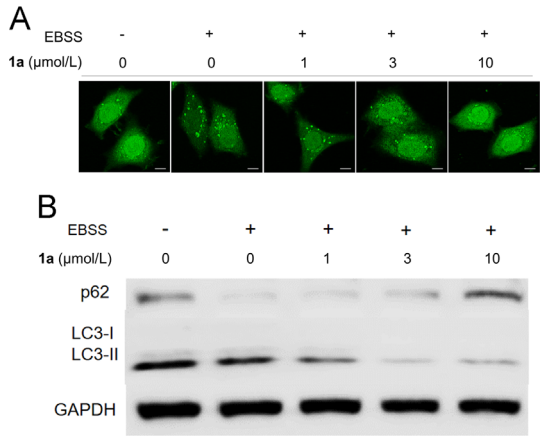

Figure 6 Aurone derivative **1a** inhibits starvation-induced autophagy in HeLa cells stably transfected with GFP-LC3 plasmid. HeLa cells were incubated with EBSS for 24 h before treated with **1a** for 24 h. (A) Cell imaging was imaged by a Leica TCS SP8 confocal laser scanning microscope system in GFP channel. Scale bar = 10 μm. (B) Cell lysis was analyzed by Western blotting.

caused by starvation or mTOR inhibition[31,32]. Before treatment with **1a**, GFP-LC3 HeLa cells were preincubated with an amino acid and growth factor-free medium (Earle's balanced salt solution (EBSS)) for 24 h to induce starvation leading to autophagy. EBSS-soaked HeLa showed the presence of GFP-LC3 spots, indicative of autophagosome formation, but these were drastically reduced by an increasing dose of aurone derivative **1a** (Fig. 6A). Moreover, the expression level of LC3-II was reduced by aurone derivative **1a** in starved HeLa cells in a dose-dependent fashion (Fig. 6B and Supporting Information Fig. S12). Rapamycin[24], a known mTOR inhibitor, was used to activate autophagy in HeLa cells. As expected, a large number of GFP-LC3 spots appeared in HeLa cells treated with rapamycin, as autophagosomes were formed (Supporting Information Figs. S13 and 14). In contrast, the formation of autophagosomes was significantly inhibited after treatment with **1a** in a dose-dependent fashion (Supporting Information Figs. S13 and 14). To further evaluate the autophagy inhibition mechanism of **1a**, HeLa cells were transfected with mCherry-GFP-LC3 plasmid, which allows monitoring of the change in fluorescence (yellow to red) as a measure of autophagic flux[33]. As shown in Supporting Information Fig. S15, the formation of autophagosomes (green dots), and clearance of autophagosomes by lysosomes (red dots) were decreased dramatically in rapamycin-induced HeLa cells after incubation with **1a**, indicating that **1a** could inhibit rapamycin-induced autophagic flux. Furthermore, we have detected the level of mTOR to further confirm the autophagic inhibition of **1a**. The results showed that **1a** had no appreciable effect on the levels of mTOR in HeLa cells (Supporting Information Fig. S16), which further indicates that aurone derivative **1a** could prevent rapamycin-induced autophagy through selectively targeting Vps34, rather than significantly regulating the levels of mTOR. Finally, transmission electron microscopy (TEM) was performed to verify the effects of aurone derivative **1a** on autophagy in rapamycin-induced HeLa cells. Representative TEM images are shown in Supporting Information Fig. S17. Typical autolysosomes induced by rapamycin were decreased dramatically after **1a** treatment in HeLa cells. Taken together, the results indicated that aurone derivative **1a** can inhibit both starvation and mTOR inhibition-induced autophagy, which we attribute at least in part to its ability to inhibit Vps34 activity *in cellulo*.

2.6. *The effect of aurone derivative **1a** on mice heart and liver*

Considering the important effect of Vps34 in the function of mammalian liver and heart, we studied the changes in heart and liver function in mice exposed to aurone derivative **1a**. Six-week-old mice were intraperitoneally injected either with vehicle (100% PEG 400) or with 60 mg/kg of **1a** every three days for 30 days. The results showed that the aurone derivative had no observable effect on both total body weight and also the weights of the heart and liver of treated mice (Supporting Information Figs. S18 and S19). Similarly, the morphology of mice heart and liver showed no obvious changes (Fig. 7A). Moreover, **1a** has no effect on the activity of alanine aminotransferase (ALT) and aspartate aminotransferase (AST), which are used to indicate liver damage or disease (Supporting Information Fig. S20). Consistent with the cellular experiments, **1a** induced the accumulation of p62 in the heart and liver without having a discernible effect on Vps34 expression (Fig. 7B and Supporting Information Fig. S21). Taken together, these data suggest that **1a** can suppress autophagy activity without damaging the heart and liver in mice. This result is significant because the genetic deletion of Vps34 induces heart and liver damage[34], and therefore aurone derivative **1a** offers a potential therapeutic option for the treatment of autophagy-related diseases without inducing cardiotoxicity and hepatotoxicity.

2.7. *Pharmacokinetic study of aurone derivative **1a***

Prior to the pharmacokinetic study of aurone derivative **1a**, the compound standard peak was determined by LC–MS/MS. The aurone derivative **1a** displayed three peaks which were confirmed as their ion fragments under MRM mode (ion-pairs: m/z 395→131; m/z 395→265) (Supporting Information Fig. S23A).

The pharmacokinetic profile of aurone derivative **1a** was studied at 2 h after compound injection by intraperitoneal injection in mice. The C_{max} value occurred between 4 to 12 h, and the maximum mean peak area (807.4 mAu) of aurone derivative **1a** in plasma was obtained at 8 h (Supporting Information Fig. S23B). However, due to the presence of isomers found in the standard aurone derivative **1a**, the actual amount of aurone derivative **1a** in

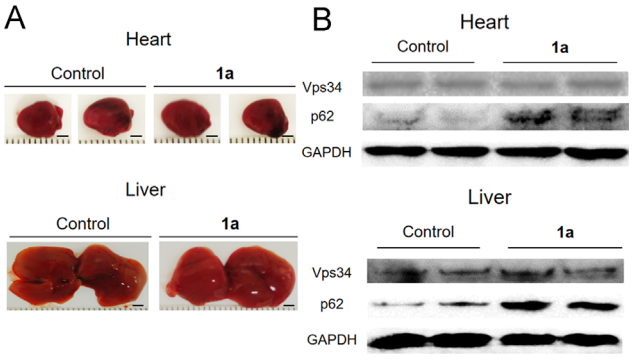

Figure 7 Effect of aurone derivative **1a** on the Vps34 in mice heart and liver. (A) Anatomical views of representative heart and liver treated with **1a**. Scale bar = 2 mm. (B) The level of p62 in mice heart and liver was detected using a Western blotting assay.

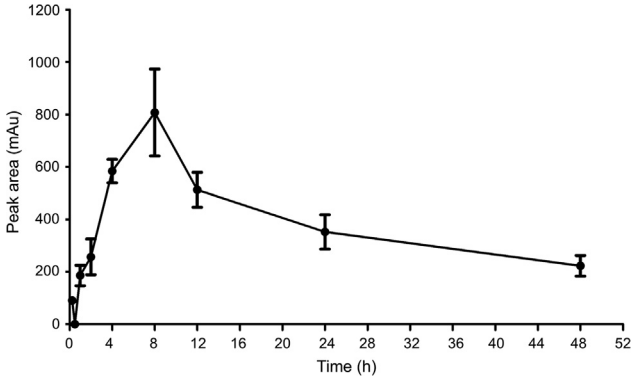

Figure 8 Pharmacokinetic profile of aurone derivative **1a**. Mean peak area of aurone derivative **1a** in blood at different time points. C57BL/6J mice were administered with an intraperitoneal injection of aurone derivative **1a** at 60 mg/kg. The concentrations of aurone derivative **1a** in the blood samples were measured at 0, 15, 30, 60, 120, 240, 480, 720 and 1440 min after administration. All data represent mean ± SEM; $n=3$.

the plasma sample could not be determined. Therefore, the pharmacokinetic profile of aurone derivative **1a** is presented as the mean peak area (mAu) at different time points in order to allow evaluation of the approximate duration and maximum concentration of the drug in the plasma (Fig. 8).

3. Conclusions

In summary, we have discovered aurone derivative **1a** as a potent inhibitor of the Vps34 activity *via* computer-based modeling of a natural products and natural product-like library. The aurone derivative **1a** upregulated p62 levels and inhibited vesicle trafficking in HeLa cells. Kinetic analysis suggested that it could function as a reversible ATP competitive inhibitor of Vps34, and is in accordance with the *in silico* modelling data showing that **1a** binds to the ATP-binding pocket of Vps34. Moreover, **1a** could prevent autophagy induced by starvation or by an mTOR inhibitor. Systemic suppression of Vps34 can cause severe cell and organ damage[34]. Pleasingly, **1a** was able to promote p62 accumulation *in vivo* without affecting the morphology of the mice heart and liver. Pharmacokinetic study of **1a** showed that the time to reach C_{max} in plasma was 8 h after single intraperitoneal administration (60 mg/kg) in mice. We envisage that aurone derivative **1a** may be harnessed as an effective scaffold for the further discovery of efficacious antagonists of Vps34 for the potential treatment of autophagy-related human diseases without inducing cardiotoxicity and hepatotoxicity.

4. Experimental

Compounds **1a**–**11** (commercial available, purity >90%) used in cell experiments were purchased from J&K Scientific Ltd.(Hong Kong, China). We synthesized and purified the aurone derivative **1a**, for the animal study. SAR405, XTT kit, Hoechst 33258, Lipo3000 transfection reagent and siVps34 were purchased from Sigma–Aldrich (Santa Clara, CA, USA). ADP-Glo™ Kinase Assay System was purchased from Promega (Madison, WI, USA). Lyso-Tracker Red was purchased from Beyotime Biotechnology (Nanjing, China). Vps34 antibody, Vps15 antibody, Beclin 1 antibody, p62 antibody, LC3 antibody and GAPDH antibody were purchased from CST (Cell Signaling Technologies, Danvers, MA, USA) and Proteintech Group (ProteinTec Group Inc., Chicago, IL, USA), respectively. All the complexes were immersed in dimethyl sulfoxide (DMSO). Further synthetic details and full descriptions of biological methods are contained in the Supporting Information Experimental Section.

4.1. *(Z)-3-0xo-2-((E)-3-phenylallylidene)-2,3-dihydrobenzofuran-6-yl cinnamate (**1a**)*

Cinnamoyl chloride (554 mg, 3.31 mmol) was added to a solution of alcohol **1d**, (880 mg, 3.3 mmol), triethylamine (370 mg, 3.66 mmol) and DMAP (36 mg, 0.3 mmol) in dry tetrahydrofuran (33 mL) at 0 °C. The solution was allowed to warm to room temperature and left to stir for 16 h. The reaction mixture was quenched with saturated NH_4Cl solution and the aqueous layer extracted with EtOAc (× 3). The combined organic layers were washed with brine (× 1) and dried over $MgSO_4$. The solvent was removed under reduced pressure to give crude target material as a yellow solid. Purification by flash column chromatography (SiO_2: EtOAc/hexanes = 1:9–1:5) gave compound **1a** as a yellow solid (581 mg, 1.47 mmol, 45%). ^{1}H NMR ($CDCl_3$, 600 MHz): δ 7.92 (d, J = 16.0 Hz, 1 H), 7.79 (d, J = 8.3 Hz, 1 H), 7.60 (dd, J = 6.9, 2.3 Hz, 2 H), 7.58–7.53 (m, 2 H), 7.44 (q, J = 5.0, 4.1 Hz, 3 H), 7.38 (t, J = 7.5 Hz, 2 H), 7.36–7.24 (m, 2 H), 7.18 (d, J = 1.9 Hz, 1 H), 7.05–6.99 (m, 2 H), 6.79 (d, J = 11.5 Hz, 1 H), 6.63 (d, J = 16.0 Hz, 1 H); ^{13}C NMR ($CDCl_3$, 150 MHz): ^{13}C NMR (151 MHz, $CDCl_3$) δ 182.3, 166.0, 164.3, 157.4, 147.8, 147.7, 141.5, 136.2, 133.8, 131.0, 129.3, 129.0, 128.8, 128.4, 127.4, 125.3, 120.4, 120.0, 117.3, 116.3, 114.4, 106.4.; IR (NaCl, neat) v: 3123, 2711, 1637, 1573, 1494, 1454, 1397, 1316, 1285, 1251, 1198, 1134, 1100, 966 cm^{-1}; HR-MS (ESI) Calcd. for $C_{26}H_{19}O_4$ [M^++H]: 395.1283, Found: 395.1280.

4.2. *ELISA assay*

ELISA assay was performed according to the assay protocol. Each well of the pre-cooled 96-well plate containing 10 μL of diluted active PIK3C3 protein, 5 μL of 125 μmol/L solution of phosphatidylinositol (PI)/phosphatidylserine (PS), 5 μL of kinase dilution buffer with 0.1% triton-100 and 100 nmol/L of a compound or 1 μL DMSO. Initiate the reaction by the addition of 5 μL of 250 μmol/L ATP solution. Sonicate the reaction mixture in the 96-well opaque plate for 10 s and continue the incubation at 30 °C for 15 min. Add 25 μL of ADP-Glo reagent to stop the reaction and deplete the remaining ATP. Shake the 96-well plate and then incubate the mixture for another 40 min at ambient temperature. Then add 50 μL of the kinase detection reagent to the each well and incubate the reaction mixture for another 30 min at the ambient temperature. Read the 96 well reaction plate using the kinaseGlo luminescence protocol on an Envision Multilabel Plate Reader (Perkin-Elmer, Waltham, MA, USA). Determine the corrected activity (RLU) by removing the blank control value for each sample and calculating the kinase specific activity.

4.3. *Kinetic assay*

Each well of the pre-cooled 96-well plate contained different concentrations of PIK3C3 protein and aurone derivative **1a**, 5 μL of 125 μmol/L solution of PI/PS, 5 μL of kinase dilution buffer

with 0.1% Triton-100. The reaction was initiated by the addition of different levels of ATP solution. The ELISA assay was then performed as above.

4.4. *Vesicle trafficking*

HeLa cells were seeded at the density of 1×10^5 cells in 96 well plate for 24 h. **1a** or DMSO was added to each well for the 24 further incubations. Cells were washed with PBS for 3 times and pretreated with Lysotracker Red (1:20,000) and Hochest 33258 (1:2000) for 15 min at 37 °C before cell imaging. The treated HeLa cells were imaged using the GE InCell Analyzer 2000 with the indicated channels.

4.5. *mTOR inhibitor induced autophagy*

GFP-LC3 HeLa cells were treated with 3 μmol/L rapamycin for 4 h in fed conditions before treated with DMSO or **1a** for 24 h. Cell imaging of HeLa cells fixed with 4% PFA were then captured using a Leica TCS SP8 confocal laser scanning microscope system in GFP channel. Or cells were collected and lysed for Western blotting assay.

4.6. *Starvation-induced autophagy*

After cultured in fed conditions or starved in EBSS for 24 h, GFP-HeLa cells were then treated for with 10 μmol/L hydroxychloroquine to terminate the autophagy. DMSO- or **1a**-treated HeLa cells were either fixed with 4% PFA and then captured in the GFP channel for cell imaging, or harvested for Western blotting assay.

4.7. *Pharmacokinetic study*

Six-weeks-old C57BL/6J female mice (body weight 25 ± 2 g) were purchased from The Chinese University of Hong Kong (Hong Kong). Aurone derivative **1a** was dissolved into 12 mg/mL in diluent buffer (PEG400:EtOH:ddH_2O = 6:1:3). Each mouse took a single intraperitoneal administration of 60 mg/kg aurone derivative **1a**. After drug administration, the blood samples were collected from the retinal vein into heparinized centrifuge tubes at appropriate intervals (0.25, 0.5, 1, 2, 4, 8, 12, 24 and 48 h). After centrifugation at $3000 \times g$ for 10 min, 100 μL of plasma was collected and stored at −80 °C until analysis. The amounts of aurone derivative **1a** in the plasma were estimated by UPLC–MS/MS analysis as described in Supporting Information. A 50 μL aliquot of plasma sample was spiked with 3.2 μL resveratrol (internal standard, 1 μg/mL). After vortexing, 300 μL methanol was added, ultrasonic dissolving and centrifuged at $9391 \times g$ for 10 min. The supernatant was collected, and then dried using nitrogen blowing instrument. The residue was reconstituted with 200 μL of methanol, and then 5 μL of the aliquot was injected into the UPLC–MS/MS system.

Acknowledgments

This work is supported by Hong Kong Baptist University (FRG2/16–17/007, FRG2/17–18/003, China), the Health and Medical Research Fund (HMRF/14150561, China), the Research Grants Council (HKBU/12301115, China), the National Natural Science Foundation of China (21575121 and 21775131, China), the Hong Kong Baptist University Century Club Sponsorship Scheme 2018 (China), the Interdisciplinary Research Matching Scheme (RC-IRMS/16–17/03, China), Interdisciplinary Research Clusters Matching Scheme (RC-IRCs/17–18/03, China), Innovation and Technology Fund (ITS/260/16FX, China), Matching Proof of Concept Fund (MPCF-001–2017/18, China), Collaborative Research Fund (C5026-16G, China), SKLEBA and HKBU Strategic Development Fund (SKLP_1718_P04, China), the Science and Technology Development Fund, Macao SAR (0072/2018/A2, China), the University of Macau (MYRG2016-00151-ICMS-QRCM and MYRG2018-00187-ICMS, China), and a Discovery Project Grant (DP160101682, Australia) from the Australian Research Council. We would like to thank Dr. Chao YANG for his kind help during in the study. We also thank Dr. Jia-Hong LU (Institute of Chinese Medical Sciences, University of Macau, Taipa, Macau, China) for providing GFP-LC3 HeLa cells.

Appendix A. Supporting information

Supplementary data associated with this article can be found in the online version at https://doi.org/10.1016/j.apsb.2019.01.016.

References

1. Murrow L, Debnath J. Autophagy as a stress-response and quality-control mechanism: implications for cell injury and human disease. *Annu Rev Pathol-Mech Dis* 2013;**8**:105–37.
2. Chen S, Dong G, Wu S, Liu N, Zhang W, Sheng C. Novel fluorescent probes of 10-hydroxyevodiamine: autophagy and apoptosis-inducing anticancer mechanisms. *Acta Pharm Sin B* 2019;**9**:144–56.
3. Kroemer G. Autophagy: a druggable process that is deregulated in aging and human disease. *J Clin Investig* 2015;**125**:1–4.
4. Nixon RA. The role of autophagy in neurodegenerative disease. *Nat Med* 2013;**19**:983–97.
5. Doria A, Gatto M, Punzi L. Autophagy in human health and disease. *N Engl J Med* 2013;**368**:1845.
6. Mizushima N, Levine B, Cuervo AM, Klionsky DJ. Autophagy fights disease through cellular self-digestion. *Nature* 2008;**451**:1069–75.
7. Bechtel W, Helmstädter M, Balica J, Hartleben B, Schell C, Huber TB. The class III phosphatidylinositol 3-kinase PIK3C3/VPS34 regulates endocytosis and autophagosome–autolysosome formation in podocytes. *Autophagy* 2013;**9**:1097–9.
8. Ouyang L, Shi Z, Zhao S, Wang FT, Zhou TT, Liu B, et al. Programmed cell death pathways in cancer: a review of apoptosis, autophagy and programmed necrosis. *Cell Prolif* 2012;**45**:487–98.
9. Russell RC, Tian Y, Yuan H, Park HW, Chang YY, Kim J, et al. ULK1 induces autophagy by phosphorylating Beclin-1 and activating VPS34 lipid kinase. *Nat Cell Biol* 2013;**15**:741–50.
10. Jaber N, Dou Z, Chen JS, Catanzaro J, Jiang YP, Ballou LM, et al. Class III PI3K Vps34 plays an essential role in autophagy and in heart and liver function. *Proc Natl Acad Sci U S A* 2012;**109**:2003–8.
11. Jaber N, Dou Z, Lin RZ, Zhang J, Zong WX. Mammalian PIK3C3/VPS34: the key to autophagic processing in liver and heart. *Autophagy* 2012;**8**:707–8.
12. Garcia-Echeverria C, Sellers WR. Drug discovery approaches targeting the PI3K/Akt pathway in cancer. *Oncogene* 2008;**27**:5511–26.
13. Morris DH, Yip CK, Shi Y, Chait BT, Wang QJ. Beclin 1-Vps34 complex architecture: understanding the nuts and bolts of therapeutic targets. *Front Biol* 2015;**10**:398–426.
14. Fleming A, Noda T, Yoshimori T, Rubinsztein DC. Chemical modulators of autophagy as biological probes and potential therapeutics. *Nat Chem Biol* 2011;**7**:9–17.
15. Miller S, Tavshanjian B, Oleksy A, Perisic O, Houseman BT, Shokat KM, et al. Shaping development of autophagy inhibitors with the structure of the lipid kinase Vps34. *Science* 2010;**327**:1638–42.

16. Pasquier B. SAR405, a PIK3C3/Vps34 inhibitor that prevents autophagy and synergizes with MTOR inhibition in tumor cells. *Autophagy* 2015;**11**:725–6.
17. Bilanges B, Vanhaesebroeck B. Cinderella finds her shoe: the first Vps34 inhibitor uncovers a new PI3K-AGC protein kinase connection. *Biochem J* 2014;**464**:e7–10.
18. Su WC, Chao TC, Huang YL, Weng SC, Jeng KS, Lai MM. Rab5 and class III phosphoinositide 3-kinase Vps34 are involved in hepatitis C virus NS4B-induced autophagy. *J Virol* 2011;**85**:10561–71.
19. Yang C, Wang W, Chen L, Liang J, Lin S, Lee MY, et al. Discovery of a VHL and HIF1α interaction inhibitor with *in vivo* angiogenic activity *via* structure-based virtual screening. *Chem Commun* 2016;**52**:12837–40.
20. Zhong Z, Liu LJ, Dong ZQ, Lu L, Wang M, Leung CH, et al. Structure-based discovery of an immunomodulatory inhibitor of TLR1-TLR2 heterodimerization from a natural product-like database. *Chem Commun* 2015;**51**:11178–81.
21. Liu LJ, Leung KH, Chan DS, Wang YT, Ma DL, Leung CH. Identification of a natural product-like STAT3 dimerization inhibitor by structure-based virtual screening. *Cell Death Dis* 2014;**5**:e1293.
22. Xiang YZ, Shang HC, Gao XM, Zhang BL. A comparison of the ancient use of ginseng in traditional Chinese medicine with modern pharmacological experiments and clinical trials. *Phytother Res* 2008;**22**:851–8.
23. Lachance H, Wetzel S, Kumar K, Waldmann H. Charting, navigating, and populating natural product chemical space for drug discovery. *J Med Chem* 2012;**55**:5989–6001.
24. Ronan B, Flamand O, Vescovi L, Dureuil C, Durand L, Fassy F, et al. A highly potent and selective Vps34 inhibitor alters vesicle trafficking and autophagy. *Nat Chem Biol* 2014;**10**:1013–9.
25. Jiang X, Bao Y, Liu H, Kou X, Zhang Z, Sun F, et al. VPS34 stimulation of p62 phosphorylation for cancer progression. *Oncogene* 2017;**36**:6820–62.
26. Duran A, Amanchy R, Linares JF, Joshi J, Abu-Baker S, Porollo A, et al. p62 is a key regulator of nutrient sensing in the mTORC1 pathway. *Mol Cell* 2011;**44**:134–46.
27. Kruidenier L, Chung CW, Cheng Z, Liddle J, Che K, Joberty G, et al. A selective jumonji H3K27 demethylase inhibitor modulates the proinflammatory macrophage response. *Nature* 2012;**488**:404–8.
28. San José-Enériz E, Agirre X, Rabal O, Vilas-Zornoza A, Sanchez-Arias JA, Miranda E, et al. Discovery of first-in-class reversible dual small molecule inhibitors against G9a and DNMTs in hematological malignancies. *Nat Commun* 2017;**8**:15424.
29. Futter CE, Collinson LM, Backer JM, Hopkins CR. Human VPS34 is required for internal vesicle formation within multivesicular endosomes. *J Cell Biol* 2001;**155**:1251–64.
30. Kang TS, Wang W, Zhong HJ, Dong ZZ, Huang Q, Mok SW, et al. An anti-prostate cancer benzofuran-conjugated iridium(III) complex as a dual inhibitor of STAT3 and NF-κB. *Cancer Lett* 2017;**396**:76–84.
31. Wei Y, An Z, Zou Z, Sumpter R, Su M, Zang X, et al. The stress-responsive kinases MAPKAPK2/MAPKAPK3 activate starvation-induced autophagy through Beclin 1 phosphorylation. *Elife* 2015;**4**:e05289.
32. Kabeya Y, Mizushima N, Yamamoto A, Oshitani-Okamoto S, Ohsumi Y, Yoshimori T. LC3, GABARAP and GATE16 localize to autophagosomal membrane depending on form-II formation. *J Cell Sci* 2004;**117**:2805–12.
33. Zhang XJ, Chen S, Huang KX, Le WD. Why should autophagic flux be assessed?. *Acta Pharmacol Sin* 2013;**34**:595–9.
34. Jaber N, Zong WX. Class III PI3K Vps34: essential roles in autophagy, endocytosis, and heart and liver function. *Ann NY Acad Sci* 2013;**1280**:48–51.
35. Zhong HJ, Ma VY, Cheng Z, Chan DH, He HZ, Leung KH, et al. Discovery of a natural product inhibitor targeting protein neddylation by structure-based virtual screening. *Biochimie* 2012;**94**:2457–60.
36. Ma DL, Chan DH, Wei G, Zhong HJ, Yang H, Leung LT, et al. Virtual screening and optimization of Type II inhibitors of JAK2 from a natural product library. *Chem. Commun* 2014;**50**:13885–8.
37. Sujatha-Bhaskar S, Huang Z, Francis G, Bryan C, Zarrin AA, Kiefer J, et al. High throughput screening of IRAK4 small molecule inhibitors in TLR ligand stimulated whole blood. *J. Immunol* 2018;**200**:174–5.
38. Leung CH, Chan DSH, Kwan MHT, Cheng Z, Wong CY, Zhu GY, et al. Structure-based repurposing of FDA-approved drugs as TNF-α inhibitors. *ChemMedChem* 2011;**6**:765–8.